INL/JOU-17-41863

Interpretation of Energy Deposition Data from Historical Operation of the Transient Test Facility (TREAT)

Mark D. DeHart, Benjamin A. Baker, and Javier Ortensi
Idaho National Laboratory

May 2017

The INL is a U.S. Department of Energy National Laboratory
operated by Battelle Energy Alliance

Interpretation of Energy Deposition Data from Historical Operation of the Transient Test Facility (TREAT)

Mark D. DeHart*, Benjamin A. Baker, Javier Ortensi

Reactor Physics Design and Analysis Department,
Idaho National Laboratory
2525 Fremont Avenue
Idaho Falls, ID 83415
* *Corresponding author: Mark.DeHart@inl.gov*

Abstract

The Transient Test Facility (TREAT) at Idaho National Laboratory will resume operations in late 2017 after a 23 year hiatus while maintained in a cold standby state. Over that time period, computational power and simulation capabilities have increased substantially and now allow for new multiphysics modeling possibilities that were not practical or feasible for most of TREAT's operational history. Hence the return of TREAT to operational service provides a unique opportunity to apply state-of-the-art software and associated methods in the modeling and simulation of general three-dimensional steady state and kinetic behavior for reactor operation, and for coupling of the core power transient model to experiment simulations. However, measurements taken in previous operations were intended to predict power deposition in experimental samples, with little consideration of three-dimensional core power distributions. Hence, interpretation of data for the purpose of validation of modern methods can be challenging. For the research discussed herein, efforts are described for the process of proper interpretation of data from the most recent calibration experiments performed in the core, the M8 calibration series (M8-CAL). These measurements were taken between 1990 and 1993 using a set of fission wires and test fuel pins to estimate the power deposition that would be produced in fast reactor test fuel pins during the M8 experiment series. Because of the decision to place TREAT into a standby state in 1994, the M8 series of transients were never performed. However, potentially valuable information relevant for validation is available in the M8-CAL

measurement data, if properly interpreted. This paper describes the current state of the process of recovery of useful data from M8-CAL measurements and quantification of biases and uncertainties to potentially apply to the validation of multiphysics methods. Our findings provide us with confidence in our methods; however, confidence and validation are not the same thing, and it is difficult to identify the data here as being useful in validation of computational methods. We conclude that in future work validation calculations must be performed in a manner similar to the actual measurements, by performing simulation of detector responses for the calibration series.

Keywords: TREAT, Calibration, M8-CAL, Instrumentation, Modeling, Uncertainty

---

1. INTRODUCTION

The Transient Test Facility (TREAT) was constructed and began operation in 1959, operating for 35 years until it was placed in a cold standby state in 1994. TREAT is in the process of being returned to operational readiness to resume transient testing, beginning with the accident tolerant fuel (ATF) campaign in the 2018/2019 time frame. Because of the greater than 20 year time span since initiation of standby status, the computational power and simulation capabilities have increased substantially since TREAT last operated and now allow for new modeling possibilities that were not practical or feasible for most of TREAT's operational history. This provides a unique opportunity to apply state-of-the-art software and associated methods in the modeling and simulation (M&S) of general three-dimensional (3-D) kinetic behavior for reactor operation, and for coupling of the core power transient model to experiment simulations.

1.1. Overview of TREAT

TREAT is an air-cooled, thermal-spectrum test facility designed to evaluate reactor fuels and structural materials under simulated nuclear excursions and transient power/cooling mismatch situations in a nuclear reactor [1]. Such testing involves placing fuel into the TREAT core and subjecting it to short bursts of intense, high-power neutron radiation. After the experiment is completed, the fuel and/or associated material is analyzed to determine the effects of the power burst. The resulting information is then used to guide the

development and improvement of advanced nuclear fuel designs, and to validate computer models of fuel and core behavior as required for U.S. Nuclear Regulatory Commission (NRC) evaluation of nuclear power reactor design and safety evaluations [2].

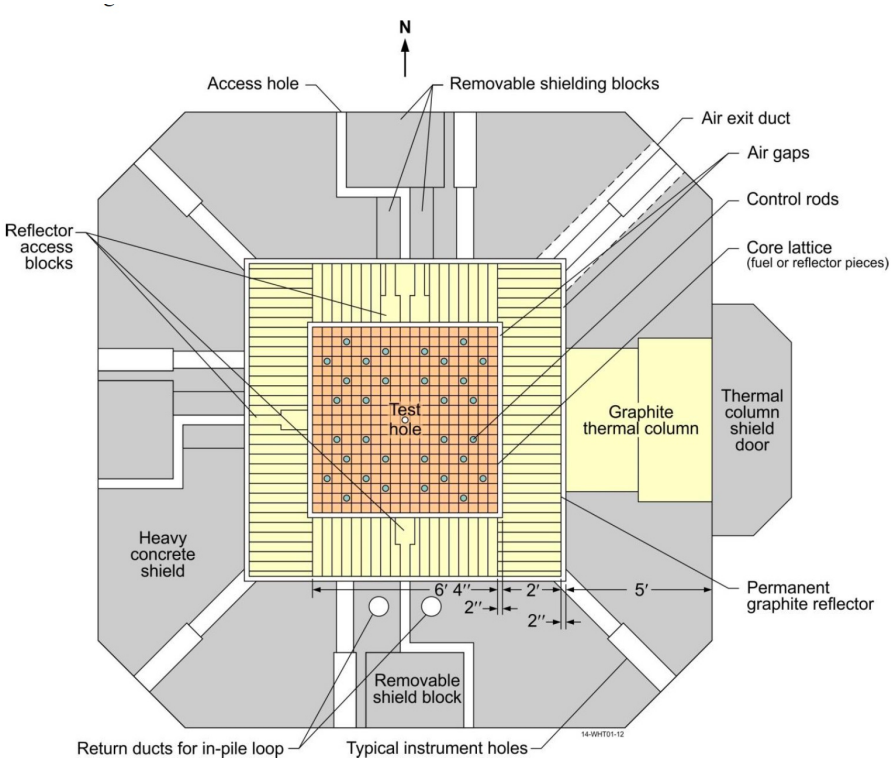

Figure 1: Top View of the TREAT core, permanent reflector, and biological shielding

The reactor is essentially a right cylindrical core within a 19×19 square lattice, loaded with fuel and reflector elements; the lattice region is fully reflected by ∼61 cm (2 ft) of graphite on all sides. In its normal operation as a pulsed engineering test reactor, there is typically a vertical central hole containing a test sample, with possibly one or more large slots running

horizontally from the core center out through the reflector. The size of the core is adjusted to provide the necessary excess reactivity to run the various transients required for test operations [3]. The reactor cavity is designed to accommodate a total of 361 assemblies arranged in a 10.16 cm (4 in) square lattice up to a maximum active core size of 193.04 cm (76 in) square by 121.92 cm (4 ft) high [1]. A top view of the core is provided in Fig. 1. Figure 2 shows a cutaway view of the full facility.

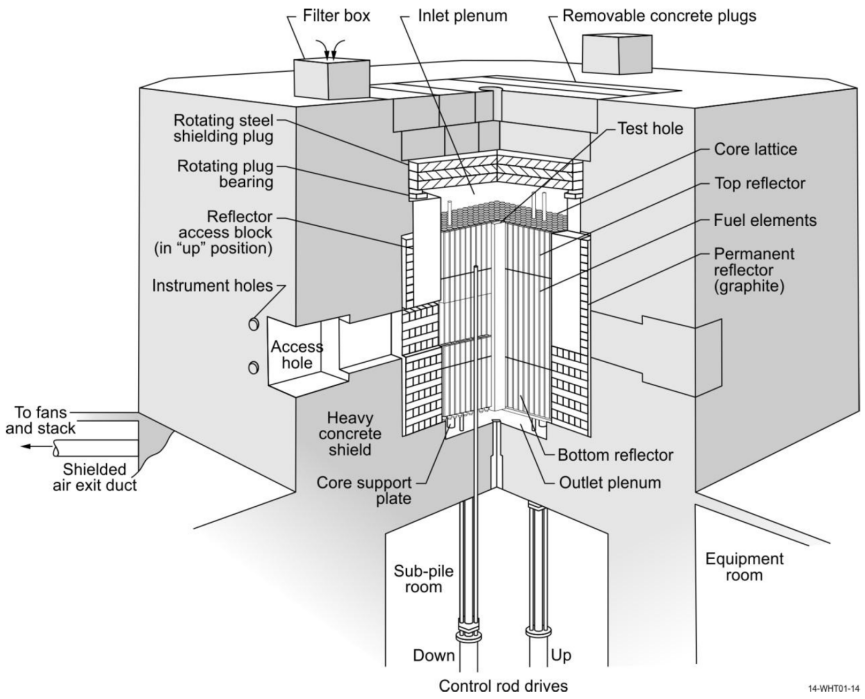

Figure 2: Cutaway illustration of the TREAT core, reflectors and biological shield, showing the numerous penetrations into the core interior

The TREAT core is driven by highlyenriched uranium (HEU) dispersed in a graphite matrix (1:10000 ^{235}U/C atom ratio). At the center of the core,

fuel is removed allowing for the insertion of an experimental test vehicle. TREAT's design provides experimental flexibility and inherent safety during neutron pulsing. This safety stems from the graphite in the driver fuel having a strong negative temperature coefficient of reactivity resulting from a thermal Maxwellian shift; this shift results in reduced fission in ^{235}U, which in turn allows increased leakage as the core heats up. This is complemented by the heat capacity of graphite, acting as a temperature sink. Air cooling is available, but is generally only used post-transient for heat removal.

1.2. TREAT Modeling and Simulation

The MAMMOTH [4] reactor multiphysics analysis application is being developed as the primary tool for TREAT M&S. MAMMOTH was developed using the MOOSE framework [5, 6], a finite element method development environment that focuses on multiphysics simulations with strongly or tightly coupled physics applications. Some of the benefits of MOOSE are parallel processing for large problems, one-, two- and three-dimensional finite element modeling support and a coherent code development environment such that any code developed by other developers will share a common framework and can be linked to one another (via shared data) within that framework. Thus, it is possible for independent physics codes to be applied as needed without special external code development to provide physics coupling. MAMMOTH is in fact a control application that inherently and seamlessly interfaces with several other MOOSE applications including Rattlesnake [7] for

solving the Boltzmann transport equation, BISON [8, 9] for heat transfer and fuel performance modeling and RELAP-7 [10] for thermal fluids calculations. MAMMOTH itself provides both macro- and micro-depletion capabilities [11]. Several preliminary studies of TREAT have already been conducted with MAMMOTH [12, 13, 14, 15, 16] .

Cross sections used for MAMMOTH simulations are currently prepared using the Serpent 2 [17] transport code using neutron cross sections based on ENDF/B-VII.1 data [18]. Serpent is a three-dimensional continuous-energy Monte Carlo reactor physics code developed at VTT Technical Research Centre of Finland. It was selected as the cross section preparation tool for this work [14] because it offers 3-D spatial homogenization and group constant generation for deterministic reactor simulator calculations. At the same time, Serpent provides a detailed reference calculation without energy, angular, or spatial discretization error. Serpent 2 also provides the ability to simulate the effect of control rod positioning and corresponding detector responses for steady state core operation.

1.3. TREAT Reactivity Computer

Parallel work supporting TREAT operations has also led to the development of a TREAT Reactivity Computer (TRC). Initially developed to test inverse-kinetics equations for a physical reactivity computer device being developed for TREAT operations, this simulator, with a graphical user interface, provides controls and readouts that a control room operator would

see during TREAT operations, converted to a multi-tab form for display on a personal computer. Figure 3 shows a portion of the interface. The simulator was built using LabVIEW 2015 [19].

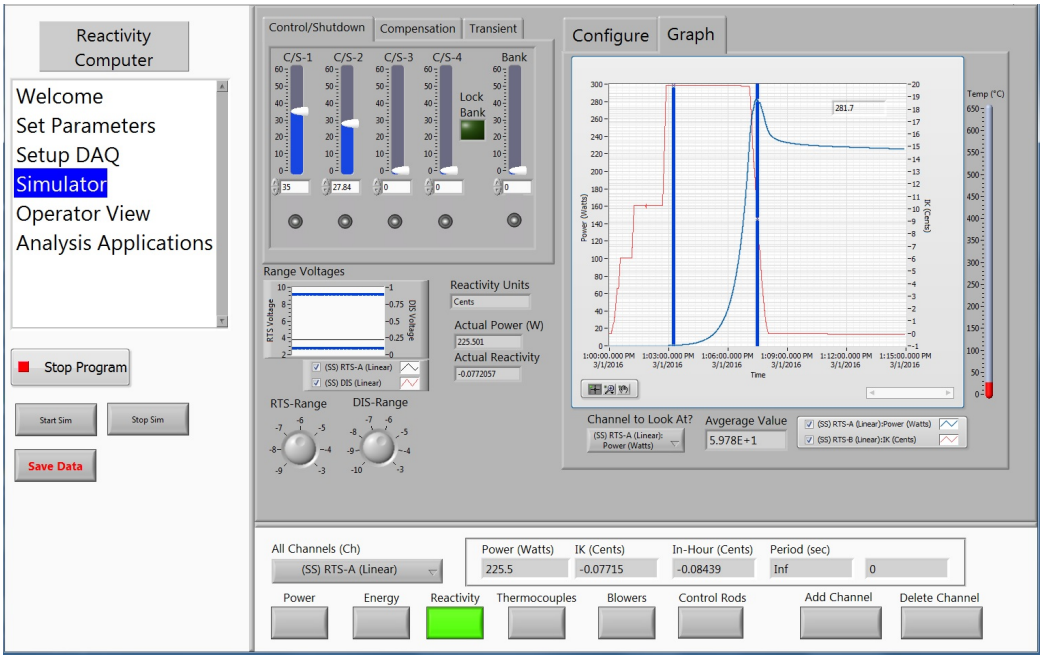

Figure 3: Graphical user interface for the TREAT Reactivity Computer

The TRC uses point kinetics for a real-time power solution but adds functionality to simulate the operation/applicability range of TREAT detectors and provides for simulation of manual operation of control rods. In essence, the simulator lets the user become the operator of the reactor. The reactivity from the control rod movements are based on historical tables generated by rod calibrations. The simulation assumes adiabatic conditions, a fuel density

of 1.72 g/cm^3, a correlation for the specific heat of the fuel:

$$C_p = -5.8219 \times 10^{-10} \cdot T^3 - 4.3694 \times 10^{-7} \cdot T^2 + 0.0028369 \cdot T - 0.01009, \quad (1)$$

where C_p is in units of J/(g-K), and the temperature of the fuel, T, is in Kelvin. We also assume a feedback coefficient of -2.2×10^{-4} Δk/k/C, where the temperature is the core-averaged temperature. These data are based on values reported for early point kinetics simulations of TREAT [3]. It is important to note that this feedback coefficient value was a derived quantity based on a reactivity measurement at with no cooling. A value of -1.3×10^{-4} Δk/k/C was determined based on the temperature change in the center of the core. Another measurement of the peak to average flux was used to correct the core-centered value to the full-core value of -2.2×10^{-4} Δk/k per average degree (C) temperature change in the core.

The general purpose of the TRC is for to allow a user to get a feel for the dynamics of TREAT operation, and to bring a sense of physicality to test data and general core behavior. It has not been formally validated in any way, but it does reproduce known transient performance, and serves as a useful aid in understanding operations. Some of the uncertainty assessments of core behaviors in following sections are drawn from TRC simulations. However, at this point this software is an in-house tool and has not been documented elsewhere, nor are there any plans for distribution.

1.4. MAMMOTH Validation

Measurements taken in previous operations (prior to 1994) were intended to predict power deposition in experimental samples, with little consideration of 3-D core power distributions. Hence, interpretation of data for the purpose of validation of 3-D methods can be, to say the least, challenging. For the research discussed here, efforts are described for the process of proper interpretation of data from the most recent calibration experiments performed in the core, the M8 calibration series (M8-CAL) [20]. These measurements were taken between 1990 and 1993 using a set of fission wires and test fuel pins to estimate the power deposition that would be produced in fast reactor test fuel pins during the M8 experiment series. Because of the decision to place TREAT into a standby state in 1994, the M8 series of transients were never performed. However, potentially valuable information relevant for MAMMOTH validation is available in the M8-CAL measurement data, if properly interpreted.

While MAMMOTH validation is the driving force for this research, this paper focuses on interpretation of data available from the M8-CAL series. To this end, Serpent calculations are used to simulate reactor operations to better understand the spatial and thermal relationships between the calibration vehicle and external detectors during operations for data collection. We also investigate measurement uncertainties to assess potential error in the measurement procedures. We begin in Section 2 by describing the nature of the data collected in those measurements and how that was used to estimate

energy deposition. In Section 3 we describe potential areas of uncertainty associated with fission measurements. Section 4 discusses M8-CAL core power measurements and their associated biases and sources of error. An example of the evaluation of biases in a subset of M8-CAL measurements by using Monte Carlo simulations is described in Section 5. Finally we summarize by making recommendations for the nature of future instrumentation and measurement approaches that are consistent with available 3-D modeling capabilities.

2. TREAT CALIBRATION METHODS

During its more than three decades of operation, TREAT provided stress testing of nuclear fuels - quick, high-energy neutron pulses that simulate accident conditions - to help the industry design even more durable fuels, establish performance limits, validate design codes, and help regulators define safety limits [2]. TREAT was designed to provide the ability to deposit a large amount of energy into an experimental sample over a short period of time. Through such a power pulse, it is possible to induce intense fission heating in the nuclear fuel being tested, to evaluate the performance of nuclear reactor fuels under severe reactor accident conditions. The reactor is also able to provide nondestructive test data through neutron radiography of fuel samples, although that was not its primary mission.

Key to understanding the behavior of fuels and structural materials during a test, and in fact a requisite of experiment design, is a quantified understanding of energy behavior in the test sample(s) during a transient test. The amount of energy deposited in an experiment during a power excuresion, along with its axial distribution, is related to a large number of factors, including but not limited to: the core configuration, the experiment vehicle design, instrumentation and containment, the nature of the fuel sample or samples themselves, coolant/moderator, control rod positions and motion history, and temperature changes during the transient. These factors are all coupled to varying degrees. With the lack of advanced 3-D modeling capabilities in earlier testing campaigns, it was not possible to predict energy

deposition in a test sample *a priori*. Hence, for most experiment series an extensive set of calibration tests was required to estimate in advance the power deposition in an experiment during a planned transient. This was used in an attempt to prevent (or ensure) the experiment crossing a given threshold, e.g., melting temperature in the fuel. Typically, a neutronically similar but simplified mock-up of the test (calibration) vehicle was used, and tests were performed with U-Zr fission wires and a fuel pin or pins matching the candidate test pin(s). Post irradiation, the samples were quickly removed from the test vessel via a separate test train and scanned or chemically assayed to determine the number of fissions that occurred in the sample. These measurements were used to determine a steady state *power coupling factor* (PCF) together with a *transient correction factor* (TCF). These two terms were then used to relate the total core energy to the energy generation in an experimental pin.

It is important to make a distinction here between calibration measurements and test measurements. Indeed, all measurements in TREAT were a form of test measurement. However, the intent of the experiment series was to study the performance of a particular fuel concept (e.g., UO_2, U metal, silicide-based clad, etc.), under specific conditions (e.g., loss of or reduced coolant flow, de-pressurization, nominal flow, boiling, etc.). However, to design the experiment, it was necessary to determine the energy generation that would occur within a pin when the transient test was subsequently run. Hence, prior to the *test* measurements, *calibration* measurements were

performed to estimate the energy generation in the test sample for a given transient pulse. This calibration series also allowed modification of the pulse shape as necessary to meet the experiment objectives. Both steady state and transient runs were performed during the calibration series in advance of the actual test series. A final set of PCF and TCF value are determined and used in the test series.

Because of the halt in TREAT operations that began in 1994, the so-called M8 transient test series never occurred. Hence, all data described here was obtained during the M8 calibration series. Hence, the PCF and TCF values were never applied to a test measurement. That being said, planned measurements during TREAT startup testing will include new determination of PCF and TCF values for the same test wire types.

PCFs were relatively straightforward to determine. Measurements were made with the core held at steady state with a low power level (80 kW for M8-CAL measurements) and at an equilibrium temperature. These were referred to as low level steady state (LLSS) measurements. The PCF has units of test sample power per gram of test sample, per unit of TREAT power, and was defined in numerous ways depending on the experiment. Generally this was in terms of the ratio of fissions or energy released in the wire or fuel pin (with some normalizing factor) to the energy in the core, typically in MJ; the definition was irrelevant as long as it was applied consistently. These definitions included:

$$\frac{fissions/g_{U_{235}}}{MJ_{core}}, \frac{J/g_{U_{235}}}{MJ_{core}}, \frac{fissions/g_{fuel}}{MJ_{core}}, \frac{J/g_{fuel}}{MJ_{core}} \tag{2}$$

The fission energy deposition was derived from post-irradiation measurement of the fission density in the sample. The core power was measured as a function of time by ion chambers located at the edge of the core and integrated to obtain the total core energy over the transient. The power coupling was determined by first measuring the fission density distribution in fresh fuel samples irradiated in TREAT under LLSS conditions. The result was then scaled to planned higher power experiment conditions using measured fission densities in fissile wires irradiated under both LLSS and higher power conditions.

Measurements were performed for the integrated number of fissions or energy in a test sample, as well as for axial distributions of power/fissions. The axial distribution could be determined by cutting an irradiated wire into a number of smaller lengths and measuring the number of fissions in each sample; the data could then be plotted to determine the axial shape as well as the location and magnitude of the fission peak. This could be used to estimate the maximum energy that could be generated within a test pin. Table 1 provides a summary of coupling factors measured in TREAT at LLSS, from Table VI of [20]. Figure 4 shows the test train design in which these measurements were made [21]. Although the drawing indicates that this is the M2/M3 calibration design, the same test train was ultimately

Table 1: M8-CAL LLSS Flux Monitor Wire Coupling Factors [20]

Item	Date	Wire ID	Core Slot	Axial Peak: Abs. f/g (x 10^{13})	Total Energy in Irrad., MJ	Measured Coupling Factor ($\frac{Peak\ f/g^{235}U}{MJ}$) (x 10^{12})	Control Rod Config.	Approximate Initial (Critical) Rod Position, in.		Wire Holder Filter
								Control/ Shutdown	Transient	
1	10/19/90	L91-8-10	Full	1.42	667	1.79	B	Fully Withdrawn	18.5	N
2	8/24/92	L91-60-1	Half	0.958	576	1.40	A	22	Fully Withdrawn	N
3	11/20/92	L91-8-1	Half	0.968	576	1.41	A	22	Fully Withdrawn	N
4	2/8/93	L91-8-6	Half	0.819	480	1.44	A	22	Fully Withdrawn	N
5	2/12/93	H91-8-1	Half	0.972	576	0.503	A	22	Fully Withdrawn	Y
6	3/2/93	L91-8-16	Half	1.26	576	1.84	B	48	11.5	N

used for calibration series M2 though M8; the complete calibration vehicle was a neutronic mockup of the Mark-IIIC transient test vehicle [20].

Note that [20] indicates that measurements for Items 1 and 6 were performed using rod configuration B, as shown in the table. However, while Control/Shutdown rods were fully withdrawn to 147.32 cm (58 in) for the first measurement, these rods were partially inserted by 25.4 cm (10 in) to the 121.92 cm (48 in) withdrawn height for the latter. Presumably, because the Item 6 measurement was performed in a half-slotted core (all fuel in the column north of the experiment removed) and Item 1 was measured in a full-slotted core (all fuel north and south of the experiment column removed), the excess reactivity in the half-slotted core may have required partial insertion of the Control/Shutdown bank of rods. For our purposes we refer to the Item

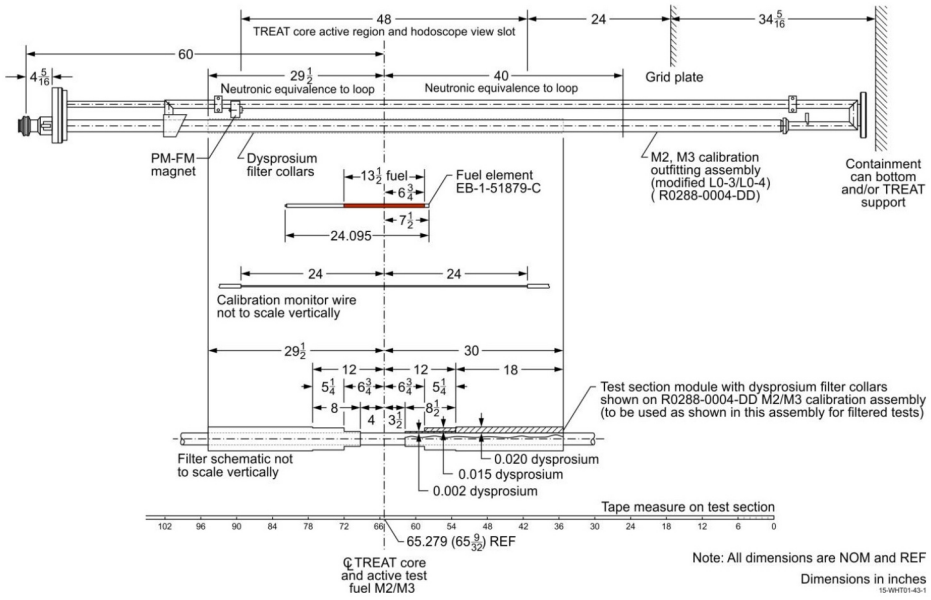

Figure 4: M2-8CAL Test Train Design

6 control rod configuration as B*.

Rod positions are indicated relative to their fully inserted position. Although the control rods themselves are identical in design, the transient rods full insertion location is higher than that of the other rod banks. Hence the withdrawal length means different relative positioning for each rod type. The full in and full out positions, along with travel lengths of each of the rod sets (transient rods vs. compensation and control/shutdown rods) are illustrated in Fig. 5.

Because of core changes during a transient (principally rod motion and changes in the neutron spectrum due to non-uniform temperature increases), the PCF changes with time. A TCF was used to correct for those changes to obtain an *effective* PCF for a fuel experiment. In order to obtain the TCF for

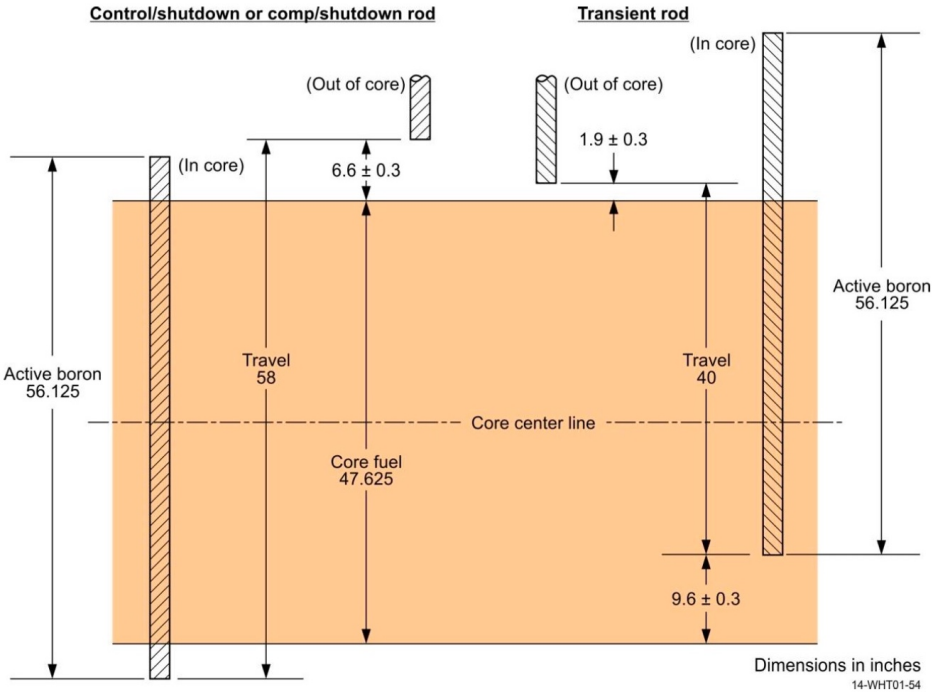

Figure 5: Schematic illustration of TREAT control rod positioning and travel lengths

a transient, it was assumed that there is a proportionality of fissions in both test fuel pins and fission wires. Zirconium alloy fission wires (also referred to as monitor wires) were irradiated in TREAT at both low-level steady state and transient conditions, and their coupling factors were obtained from analysis of the number of fissions that occurred and measurements of the total core power. Typically low enrichment wires were used, although high-enrichment fission wires could be used if enclosed in an appropriate neutron filter (the goal was to prevent the wires from melting during a transient calibration test). Item 5 in Table 1, ID H91-8-1, was a high-enrichment wire enclosed within a dysprosium collar. This configuration resulted in the

significantly reduced PCF reported for this wire.

Because of differences in compositions, enrichment and size, the PCF for fission wires were different than those of the fuel pins. Nevertheless, it was assumed that the *ratio* of the coupling factor under transient conditions to the coupling factor at LLSS for the wires is the same as that for the test fuel pin (operating experience indicated that this was a reasonable assumption):

$$\frac{PCF_{pin,transient}}{PCF_{pin,LLSS}} = \frac{PCF_{wire,transient}}{PCF_{wire,LLSS}}. \tag{3}$$

At this point, $PCF_{pin,transient}$ is not known; the subject test pin will be irradiated under transient conditions when the actual post-calibration testing is performed. Thus it is the quantity that needs to be estimated in the calibration tests to prepare for full power excursions. Thus, rearranging the terms from Eq. 3:

$$PCF_{pin,transient} = PCF_{pin,LLSS} \cdot \frac{PCF_{wire,transient}}{PCF_{wire,LLSS}} \tag{4}$$

or

$$PCF_{pin,transient} = PCF_{pin,LLSS} \cdot TCF. \tag{5}$$

Recall that from Eq. 2 that PCFs are expressed in terms of the energy deposited in a sample divided by the total energy produced within the core. If E_{pin} is the energy that will be deposited in a fuel pin in an actual test, and E_{core} the total core energy release for a transient, then

$$PCF_{pin,transient} = \frac{E_{pin}}{E_{core}}. \tag{6}$$

Substituting the right hand side of Eq. 6 for the left hand side of Eq. 5 and moving E_{core} to the right hand side, we have

$$E_{pin} = E_{core} \cdot PCF_{pin,LLSS} \cdot TCF, \tag{7}$$

which is typically written as simply

$$E_{pin} = E_{core} \cdot PCF \cdot TCF. \tag{8}$$

If the same method was used to estimate the power at steady state and during transients, then the accuracy of the exact power determination was not important; errors would cancel in the corresponding PCF terms. However, for consistency in the core conditions and to minimize instrumentation drift, efforts were made to perform all calibration measurement in the shortest practical time period. If (1) careful calibration measurements were taken, (2) the assumption of Eq. 3 was valid and (3) the test transient had exactly the same response as the transient calibration tests, then knowledge of the integrated core response during a transient was sufficient to predict the energy generation in a test fuel pin. If it was also assumed that the TCF is approximately constant with time, then the time-dependent energy generation is also known:

$$E_{pin}(t) \approx E_{core}(t) \cdot PCF \cdot TCF. \tag{9}$$

The M8-CAL measurement methods and results provide one of the most complete sets of measurements for use in computer code validation [22] and was selected for use in validation of transient calculation methods, specifically for MAMMOTH validation. However, one of the challenges in validating computer codes against measured data is that there are unavoidable uncertainties in the data. In order to best compare computed values with measured values, the method for measuring the data must be understood, along with the potential biases and sources of uncertainty. Further, when possible, it is best practice to perform calculations in a similar manner to that in which the measurement was performed.

The following sections seek to describe the current state of knowledge of the actual M8-CAL PCF/TCF measurements, both steady state and transient, and to provide insight into the potential sources and magnitude of uncertainties. In Section 3 we consider quantities related to the test samples. In Section 4 we examine uncertainties and potential biases associated with the measurement of reactor power during corresponding tests.

3. SOURCES OF UNCERTAINTY IN FISSION MEASUREMENTS

3.1. Sample Mass or Isotopic Content

The mass of sample wire or fuel within a pin should be able to be determined with a great deal of accuracy; if fissions are normalized to an isotopic or elemental composition, both the mass and enrichment/mass fraction must also be determined. From historical documentation, mass is typically reported with an uncertainty. However, information on isotopic and/or mass fractions (e.g., 0.711 at.% ^{235}U in a U-Zr alloy with 10 wt.% zirconium or UO_2 enriched to 4.5%) are not always available, so the uncertainty in the calcation of an isotopic content can be difficult to determined and must be conservatively assumed. For M8-CAL measurements, analytical chemistry results were provided for three different wire samples taken from the same batch as the calibration wires. ^{235}U enrichment was measured as 19.833 $\pm$ 0.005 wt.%; the uranium content within the wires was measured at 6.007 $\pm$ 0.003 wt.%. However, while isotopic compositions are reported for three fuel pin types used in the calibration series, these numbers are not provided with uncertainties, and vary slightly from those reported elsewhere for the same fuel types.

In addition, since the primary goal of the PCF is to establish the relationship of the core power to the energy being deposited in a test sample, one has to determine if the basis for the mass unit should be the fissile material (if that is the source of the majority of the energy) or if the additional materials in the sample have enough gamma and neutron heating to warrant

consideration.

3.2. Determination of the Number of Fissions in a Sample

In order to estimate the number of fissions produced in a flux wire or fuel pin, for the M8-CAL test series the general procedure was to irradiate the sample then remove from the core, tranfer to the counting facility and measure the number of gammas being produced from the 1.5916 MeV photopeak from ^{140}La using a Ge(Li) detector. A relative axial distribution would be produced by cutting a flux wire into ∼1.25 cm samples and counting gammas for each sample. Of course, each sample would need to be accurately weighed to calculate fission densities in each location. But this approach only provides relative fission rates. Thus some of the wire segments were chemically assayed in order to obtain an absolute activity. From this activity the actual number of fissions could be calculated.

Knowledge of this process allows us to identify some of the potential uncertainties by reviewing the theory of the measurement. We begin with the gamma measurement. ^{140}La is produced as a fission product and has a 1.678 d half-life. As such we can use the activation/decay equation to describe its production in a reactor:

$$dN_n(t)/dt = \varepsilon_n R(t) - \lambda_n N(t), \tag{10}$$

where:

n is the nuclide of interest, ^{140}La,

$N(t)_n$ is the total number of ^{140}La nuclei in a sample,

ε_n is the fission yield of ^{140}La,

λ_n is the decay constant of ^{140}La,

and $R(t)$ is the fission rate in the sample $= \phi\Sigma V$, where:

ϕ is the neutron flux,

Σ is the macroscopic cross section for fission (in this case ^{235}U),

V is the volume of the sample.

Under LLSS conditions, the flux in Eq. 10 will be constant (ignoring startup/shutdown ramps); hence the production term is also constant. It is further assumed that there is no significant inventory of ^{140}La before irradiation. The equation describing the activity during the irradiation then simplifies to:

$$A_n(t_1) = R_n(1 - e^{-\lambda_n t_1}), \tag{11}$$

where t_1 is the irradiation time, and $R_n = \varepsilon_n R$, the production rate of ^{140}La. Post irradiation,

$$A_n(t_2) = A_n(t_1)e^{-\lambda_n(t_2 - t_1)}, \tag{12}$$

where t_2 is the time after shutdown at which the measurement is made.

Since ^{140}La has a long half-live (1.678 d) relative to the irradiation time ($\sim$2-3 h), the $\lambda_n N(t)$ term in Eq. 10 may be been neglected. In this case, the equation reduces to:

$$A_n(t_1) = \frac{R_n t_1}{\lambda_n}. \tag{13}$$

The experiments are then counted some time after removal from the core, t_2 to determine the number of photons in the 1.5916 MeV photopeak. The number of counts are divided by the count period, the efficiency of the detector and any other needed conversions (e.g., branching ratio of gammas) to establish the activity of the ^{140}La at the moment of the count. This activity can then be extrapolated back to the point at which the irradiation ceased and is used to infer the total number of fissions per second at the irradiation power. The length of irradiation is multiplied to the fissions/second to obtain the total number of fissions during the run.

$$A(t_1) * t_1 \sim fissions \tag{14}$$

Hence, potential sources of error come from (1) possibly neglecting decay during irradiation, (2) non-constant power ramps during startup and shutdown, (3) irradiation timekeeping, (4) decay timekeeping, (5) counting statistics and (6) detector efficiency. We examine each of these uncertainties below.

3.2.1. Neglecting Decay During Irradiation

Based on the M8 calibration report it is unknown if the reported fissions/gram during irradiation took into account the decay of the ^{140}La during the irradiation. Since most of the irradiations were on the order of 2-3 h we

can estimate that the potential error to the reaction rate term to be ∼1.7 - 2.6%. However, this is a trivial calculation and was most likely included.

3.2.2. Ramp-Up / Ramp-Down Power

The theory generally used for isotope irradiation assumes a constant flux over the time of irradiation and ignores the fact that the experiment is being irradiated before the reactor reaches the irradiation power level and when the reactor is being shut down. The integral flux during the ramp-up to power and the ramp-down is usually small in comparison to the integral steady-state flux and is usually ignored.

To get an idea of how much integral energy there might be in a TREAT run, a simulation was performed using the TRC described in Sect. 1.3, where manual controls were used to bring the reactor up to power as fast as possible and maintain the power for a two hour irradiation. The irradiation was modeled after the H91-8-1 HEU wire irradiation from the M8-CAL series [20]. The simulator operator was able to sustain a ramp-up with reactivities up to 50 cents, reduced as the desired power was reached. The ramp-up energy consisted ∼1% of the total energy and the ramp-down (scram) <0.05%. Hence, the actual energy deposition would be approximately 1% greater than the at-power energy deposition.

We have not been able to locate historical documents providing the digitized TREAT power history for LLSS irradiations. It appears that the only recorded data was during the transients. Even without the power history en-

gineers could have estimated the energy during the ramp-up/ramp-down to improve the results, or given its magnitude they may have ignored it. However, documentation does not provide information on the approach taken.

3.2.3. Timekeeping During Irradiation

Without a power history with which to verify, the analyst must rely upon the operator-reported start and stop times. When an operator approaches the desired power level, the point at which they officially record the starting point could change from operator to operator. One operator may start the clock when they are within 10kW of the desired power since an appreciable amount of fissions are being produced in comparison to the fissions at the desired power level. Another operator may take a several minutes to rebalance the rods and stabilize to power level before recording the start time. Or the time at which the reactor is actually started up at the beginning of the power ramp-up may have been written down. In any of these scenarios, the error is proportional to the length of the entire irradiation. The best practice would be to immediately start the clock when the reactor is near the desired power level because during this time the number of fissions becomes important. Because scram is immediate, it is likely there would be little uncertainty associated with the time recorded, perhaps on the order of a few seconds, and this can be neglected relative to the startup time to critical.

If it were to require 15 minutes for an operator to stabilize the rods before declaring the steady-state power had been reached, the error could

be rather substantial. For the case of a two hour run the error would be $\sim(15/(120+15)) = 11.1\%$.

3.2.4. Timekeeping After Irradiation

The time used to back-compute the activity from the time of a counting measurement to the time at which the irradiation ceased (reactor was scrammed) is dependent on the clocks used. There can be errors between clocks if two clocks are used and they are not syncronized. Historically, counting was performed at a counting facility outside of TREAT, presumably with a different clock. However, the sensitivity to time measurements during decay would be much less than that of irradiation because the error will be associated with the ^{140}La half-life of 1.678 d. An error of ten minutes between clocks would result in 0.3% error in the calculated activity, and such a large discrepancy is unlikely.

Again, without a power history or knowledge from the procedures or analysis documents it is impossible to know how much the error is in reported time values, which leads to additional uncertainty in the estimated magnitude in fissions/gram in the sample.

3.2.5. Counting the Photopeak

The uncertainty in the number of counts goes as the square root of the counts. As a standard practice measurements are usually designed to exceed 10,000 counts, for which there is 1% standard deviation on the mean value. Counting statistics should not have been a problem as long as (1) sufficient

integral counts were measured and (2) issues like pulse pileup for high activity samples were avoided. For low-activity samples, where the counting period is sufficiently large (i.e., several hours) relative to the half-life, then corrections must be made to account for the changing activity during the count.

3.2.6. Detector Efficiency

Measurement experience dictates that the most probable cause of error during counting is the efficiency of the germanium detector. Typical relative efficiencies are ~0.3 for Ge(Li) detectors in the 1 MeV range, which correspond to $\sim 10^{-4}$ photons being detected per photon entering the detector. Because this is such a low value, small changes in magnitude can change the estimate for the absolute activity by several percent.

3.2.7. Estimation of Net Error

The reported uncertainty in the number of fissions/gram in the M8 calibration report is 2.5% for the measured absolute values and 5% in the relative values. It is unknown what categories these uncertainties enveloped but it is suspected that they only encompass the uncertainties in the counting process and exclude the uncertainty for timekeeping in the irradiation process.

Table 2 summarizes the approximate magnitudes of the highlighted sources of uncertainty in the measured fissions/gram value. With no other source of information, it is probably safe to assume that the reported values for fissions/gram in the sample have uncertainties of on the order of 5%.

Table 2: Estimated Uncertainties in the Reported Sample Fissions/Gram Value.

Source of Uncertainty	Estimated Effect (%)
Neglecting Decay During Irradiation	1.7 - 2.6
Ramp-Up Power	1
Ramp-Down Power	$<<1$
Timekeeping During Irradiation	0 - 11
Timekeeping After Irradiation	<1
Counting the Photopeak	<1
Detector Efficiency	2-5
Estimated Net Uncertainty	~ 5

4. DETERMINATION OF CORE POWER

The largest sources of error in the determination of power coupling factors are known to originate from the determination of reactor power. To understand these sources of error we must first understand how the TREAT core power is measured.

In order to calibrate the detectors for power measurements, a heat balance is performed in TREAT by measuring the temperature change in air forced through the core at power. The TREAT fuel assembly design features chamfered corners, which form diamond-shaped passageways for forced flow of cooling air (provided by two blowers) which travels downward axially from the top of the core. The flow channels are illustrated in Fig. 6, which shows nine chamfered fuel elements surrounded by air flow regions between elements and at chamfered corners. The blowers produce a combined flow rate of up to 85 m^3/min (6000 ft^3/min). Typically the blowers are used to remove stored energy from the reactor after a transient, but they were also used for heat balance measurements. To perform such a measurement, the two blowers were turned on and the reactor operated at steady state for a few hours to come to thermal equilibrium. The temperature from the inlet/outlet air is used along with barometric pressure and air flow rate to determine the power being produced by the reactor.

Neutron ionization chamber detectors used in TREAT produce a current in relation to the flux that they are exposed to, by means of a $^{10}B(n,\alpha)$ reaction. When the reactor reaches its steady-state equilibrium temperature,

the current from the chambers is assumed to represent the energy measured in the heat balance. In previous calibration campaigns operators would also adjust the detector position (distance from the core) to modify the current from the detector to equal some desired value. It was then assumed that the detector response was linear with power. The chambers were then used to specify the power level after the heat balance for each campaign.

In TREAT there are three chambers reporting energy during a operation and 14 chambers that report the instantaneous power level. However, there are different regimes in which different chambers operate. Additionally, several of the instrument holes house two chambers that are side by side (A & B positions) on a carriage that can be moved forward and backward by rotating

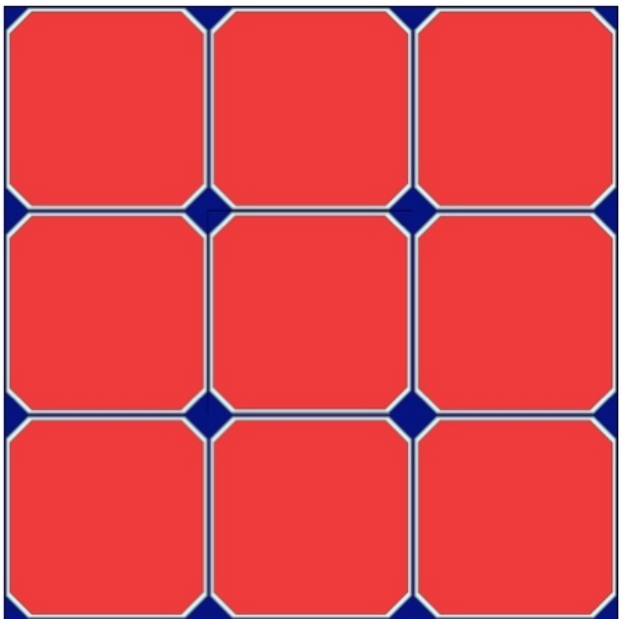

Figure 6: Configuration of fuel elements and air channels within the TREAT core

an external positioning knob. The chamber used to report the power for the LLSS irradiations is known as the *DIS-Linear chamber*. The detectors are identified and located as described in Tables 3-5. The location of each of these positions is illustrated in Fig. 7, where north is located at the top of the figure. All detectors located in the *Upper* slot are positioned 30.5 cm (12 in) above the core centerline, while *Lower* detectors are positioned 30.5 cm (12 in) below the core centerline.

The central square region in the figure, containing a 19×19 square lattice, is the graphite core; the experiment is located in the center of the core. The region from the central experiment region to the north (up) is typcially unfueled and provides an air slot toward the fast neutron hodoscope located outside the core [23] (see also Fig. 2). Most M8-CAL measurements were performed with the half-slotted configuration, although some of the initial measurements were performed with all fuel elements replaced with unfueled *slotted* element along the same north to south column for the full-slotted configuration. The region outside the core is a permanent graphite reflector. The outermost octagonal region is a concrete biological shield. Steady state detector positions are represented as dark rectangular bodies located adjacent to the core on the west and south faces of core, inside the permanent reflector; these locations are close to the core to detect sufficient flux levels during low power operation. Transient detectors are positioned in the four corners, within the biological shield but outside the permanent reflector. These locations were selected to reduce the possibility of saturation during

high-power pulses. Detectors could be moved farther from the core or a filter placed in front of or around the detector as needed. Each detector region shown in the figure actually contains the two A and B position detectors described in Tables 3-5. Note that the detector slot on the northern face of the core is not currently being used. It should also be noted that the biological shield to the east of the core is filled with graphite to provide a thermal column, although there are currently no plans to use this capability.

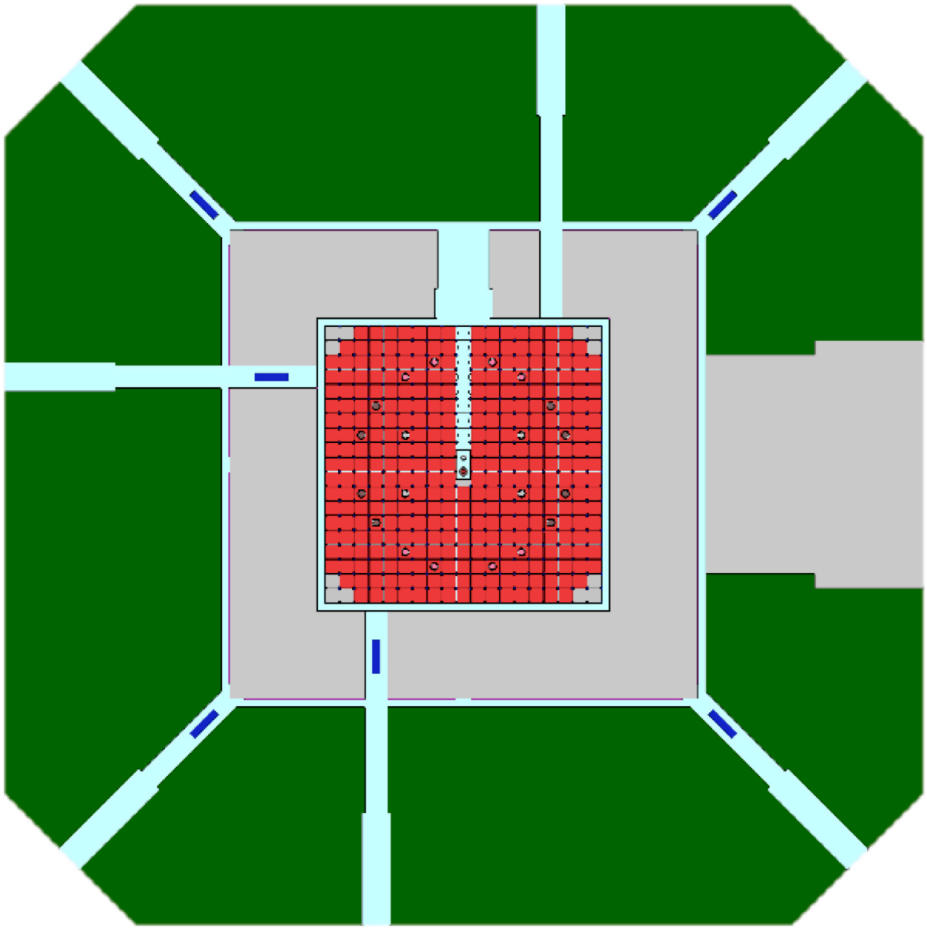

Figure 7: Location of TREAT core detectors

Table 3: TREAT Steady State Ionization Chambers

Identification	Short Name	Location
Steady State Linear A	SS-Linear-A	West Face Lower, Position A
Steady State Log/Period A	SS-Log/Period-A	West Face Lower, Position B
Steady State Linear B	SS-Linear-B	South Face Lower, Position A
Steady State Log/Period B	SS-Log/Period-B	South Face Lower, Position B

Sources of measurement uncertainty in the power reading from the various detectors come from (1) heat balance measurements, (2) transient detectors being in lower ranges during calibration, (3) human control, (4) temperature and (5) control rod configurations [24, 25]. The following subsections provide details on each of the potential sources of uncertainty.

4.1. Heat Balance

Because TREAT is not pressured or sealed, and the number of removable/reconfigurable slots around the core, air was known to leak into the core; approximately 30% of the flow could be from air in-leakage. Some of the penetrations and air leakage routes can be deduced from Figs. 2 and 7. This was reported to change the heat balance measurements by as much as ∼10% [26] as a result of thermal stratification in the building, due to in-leakage air being cooler than the air inlets above the core. To alleviate this problem, heat balance measurements were eventually performed with all external openings sealed by tape or appropriate backfill to minimize air leakage; this provided a significant improvement but could not eliminate all leakage. However, Ref. [26] indicates that a "method of measuring TREAT

Table 4: TREAT Transient Ionization Chambers

Identification	Short Name	Location
Transient Linear A	Linear-A	Northwest Upper, Position A
Transient Energy A	Energy-A	Northwest Upper, Position B
Transient Log/Period A	Log/Period A	Northwest Lower, Position B
Transient Linear B	Linear-B	Southwest Upper, Position A
Transient Energy B	Energy-B	Southwest Upper, Position B
Transient Log/Period B	Log/Period-B	Southwest Lower, Position B
Transient Linear C	Linear-C	Southeast Upper, Position A
Transient Energy C	Energy-C	Southeast Upper, Position B
Transient Log/Period C	Log/Period-C	Southeast Lower, Position B
Automatic Reactor Control System Linear	ARCS-Linear	Northeast Upper, Position A
Automatic Reactor Control System Log/Period	ARCS-Log/Period	Northeast Upper, Position B

reactor air-inlet flow using a portable turbine-type flowmeter, although not resulting in measurements of accurate magnitude, is repeatable and scaleable to TREAT's measured flow rates." After about 1980 corrections had been made to flow rates, reducing measured flow rate errors to less that 4.8% [26]. However, heat balance measurements would still be influenced by air stratification within the building, which could be significant on extremely hot or cold days.

The fact that a steady state condition was assumed for the measurement could also introduce error. When a heat balance run was performed it would take considerable time for the core to heat up to the equilibrium state, where air is removing the same amount of energy as is being pro-

Table 5: TREAT Startup Ionization Chambers

Identification	Common Name	Location
Dedicated Information System Startup A	DIS-Startup-A	West Face Upper, Position A
Dedicated Information System Linear	DIS-Linear	West Face Upper, Position A
Dedicated Information System Startup B	DIS-Startup-B	South Face Upper, Position A

duced. Written records for one heat balance indicated six hours and forty minutes at power before equilibrium was assumed (see the test data record for this heat balance run provided in Fig. 8) If the reactor was not allowed to operate for the requisite time the reported power would underestimate the true power. Asymptotic exit air and fuel thermocouple readings were used to judge the approach to equilibrium, but temperature can change very slowly in a graphite core, making the determination of steady state difficult to judge. To compound this issue, because of the temperature increase and the corresponding loss of reactivity during heat-up, control rods were continually moved. Control rod withdrawal would change the power distribution in the core, which in turn would change the temperature distribution.

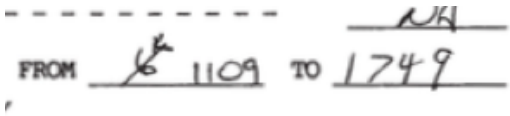

Figure 8: Handwritten record of TREAT operation time for a heat balance measurement from 1990.

Based on simulations of adiabatic core heating and measured data (the scope of which is beyond this paper), we judge that heat balance measurements are able to reach within roughly 0.5% of the final temperature after

$\sim$7 h at power, and the subsequent translation to power (described below) is probably near 1%. This is based solely on engineering judgment given the limited available data. However, this estimate is based on the final temperature and control rod configurations for this measurement, and may change under different conditions.

The correlation used for the converting the temperature change in air flowing past the core during heat balance measurements has changed over the years. At the time of the M8-CAL power measurements, the following empirical relationship was used to estimate the steady state core power, P_{core}:

$$P_{core} = 2.221 \times 10^{-3} \Delta T_{core} F \sqrt{\frac{p_{out}}{273.16 + T_{out}}}, \tag{15}$$

where:

T_{out} is the air outlet temperature (C),

p_{out} is outlet pressure (psia),

ΔT_{core} is the air temperature rise (C), and

F is the flowmeter reading (cfm).

Unfortunately, having no data available to be able to assess this accuracy of and variations from this empirical relationship, it is difficult to assign a meaningful uncertainty.

4.2. Transient detector calibration

The transient ionization chambers are calibrated at the same time as the steady state chambers. However, at LLSS the detectors are operated

within the lowermost of the applicable ranges for the detectors. This means that there is more variation due to noise in these ranges, and requires the assumption of a linear response as a function of the various detector range settings. Again, we do not have enough information to assess uncertainties, although we are confident that this approach introduces a non-neglible error.

4.3. Human Control

As discussed in Section 3.2.2, a constant flux for an experiment irradiation is usually assumed. It is known that the operators had to maintain the reactor power manually during these irradiations and the rods moved by ∼11.5-16.5 cm (4.5-6.5 in), or ∼1/10th of the full rod motion during irradiation to offset temperature feedback effects. The control rods induce a very large source of uncertainty in the power measurement and will be discussed in the following sections. However, this would mean that the operators had to constantly adjust rods, which would produce small changes in the reactor power. Using the TRC simulator with manual controls, a simulation was used to illustrate this principle. Figure 9 shows of the power history when the simulator operator was assigned to take the core to 80kW and maintain that power level for two hours.

From the simulation the mean value for the run was really 80.657 kW with a standard deviation of 1.371 kW, with maximum and minimum powers of 86.4 and 72.9 kW, respectively. The result was a difference of ∼0.82% in the power level due to operator control. This value is subjective based on the

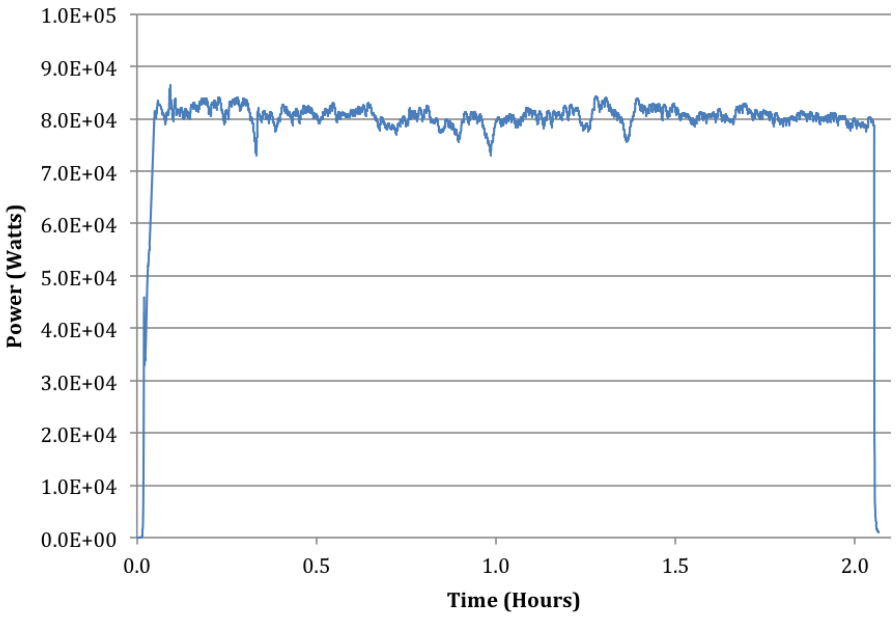

Figure 9: Power trace from INL TREAT simulator with operator required to bring core to 80 kW and maintain the power level for two hours

operator and their reactor operations skill level. It is therefore assumed that a good operator should be able to maintain the mean power level at within 0.5-1.0% of the indicated power.

4.4. Temperature Influence on Detectors

It has been shown [24] that the core temperature can influence neutron detectors in a manner such that they report a power than is different from the actual core power. As the core heats up it requires a higher neutron flux to maintain the same power level. Hence, the flux seen at the detector itself is dependent on the core temperature. It is reasonable to assume that the TREAT ionization chambers will underestimate the power when the

core temperature is below that of the detector calibration measurement, and conversely, the detectors will read too high when the temperature exceeds the detector calibration temperature. This of course would be more complex during a transient, when temperature changes lag flux changes due to stored heat effects in the core graphite.

Serpent 2 calculations were performed to evaluate the effect of (a) core temperatures and (b) control rod configurations on detector readings. Beginning with temperature effects, calculations were performed for temperatures of 294K (nominal room temperature) and 700K (estimated maximum average temperature). The Serpent simulations used 2.5×10^{10} neutron histories to reduce errors for the transient detectors, which are located farthest from the core and most difficult to tally (see corner detector locations in Figure 7). Track length estimator detectors available in Serpent were used to improve the efficiency of tally estimates.

Changes in the detector responses as a function of temperature are show in Tables 6 and 7 for a fixed power level. These are tallies by detector location, not a simulation of specific detectors, hence only the detector location is listed in the table.

As can be seen from the tables, the temperature-dependent changes for face positions (used in LLSS calibration meaurements) is on the order of 20% over this temperature range, while transient detectors are affected by on the order of 9% for the same temperature change. While it is possible that the decrease in sensitivity to temperature dependence may result from

Table 6: Calculated Percentage Changes in Startup/Steady State Detector Responses for Temperature Chanages Between 294K to 700K at a Constant Power

Startup & Steady State Detector Locations	Percentage Change	Net uncertainty (%)
West Face, Upper Position	20.52	0.04
West Face, Lower Position	20.58	0.04
South Face Upper Position	19.16	0.04
South Face Lower Position	19.73	0.04

Table 7: Calculated Percentage Changes in Transient Detector Responses for Temperature Chanages Between 294K to 700K at a Constant Power

Transient Detector Locations	Percentage Change	1σ uncertainty (%)
NW Corner, Upper Position	9.05	2.56
NW Corner, Lower Position	9.17	2.57
NE Corner, Upper Position	4.76	2.42
NE Corner, Lower Position*	6.09	2.45
SW Corner, Upper Position	7.76	3.37
SW Corner, Lower Position	12.27	3.60
SE Corner, Upper Position	9.43	3.48
SE Corner, Lower Position	9.41	3.47

*No detectors are currently located in this position.

distance, the transient detectors are also surrounded by 30 mils ($\sim$0.0762 cm) of cadmium so a direct comparison is difficult. When the same cadmium filters are added to the west face upper location (position of the DIS-Linear chamber used for LLSS calibration), the temperature sensitivity is reduced to $\sim$8.5%, a little less than half of that reported in Table 6. Hence, with a cadmium cover simulated on all detectors, the ion chamber responses are about the same. Certainly no conclusions can be drawn on the effect of location, but it is clear that temperature does have an effect on transient

detectors.

Overall, we can expect the uncertainty in the reported power from a calibration measurement to be on the order of **up to** ±20%, depending on the state of the reactor in comparison to the point in which the chambers were calibrated. It is expected that the error is much less with core-average temperatures ∼400K, since the heat balance temperature should have been in this range. The LLSS irradiations used to determine initial wire and fuel pin PCFs should have had similar states to those used in the calibration and the changes to the reported power level are expected to be <5-10% for those measurements.

4.5. Control Rods Effects

TREAT has three sets (banks) of control rods: Compensation, Control/Safety and Transient rods. Figure 10 shows the locations of the rods. Compensation rods are located closest to the experiment, would have the strongest effect on that experiment, and thus are always fully out for transient. The Transient rods are partially inserted for desired Δk upon full withdrawal, then rapidly fully withdrawn to initiate a transient. The Safety/Control rods are partially inserted to bring the core to a critical state prior to the transient. Each rod is located within an annular tube inset within a fuel element; a graphite follower is below the poisoned length of each rod. Figure 11 shows a portion of the TREAT core centered on a control element, from a detailed Serpent 2 model of TREAT.

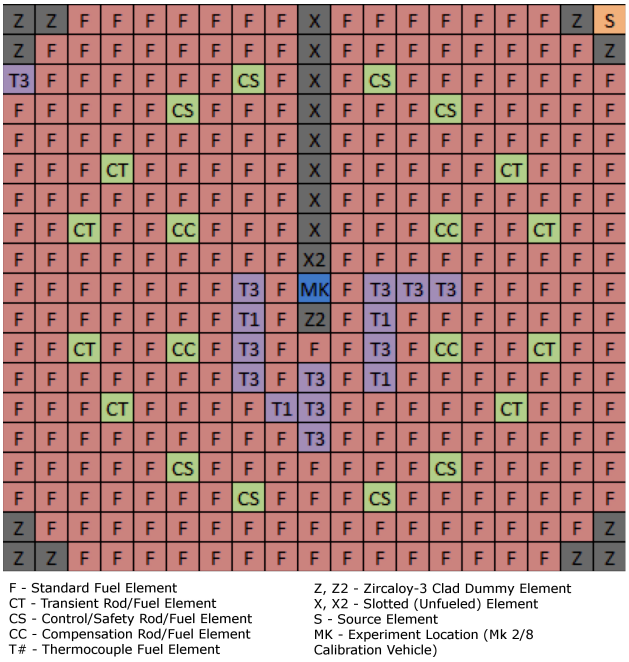

Figure 10: Location of the three sets of control elements within the M8-CAL core configuration [21].

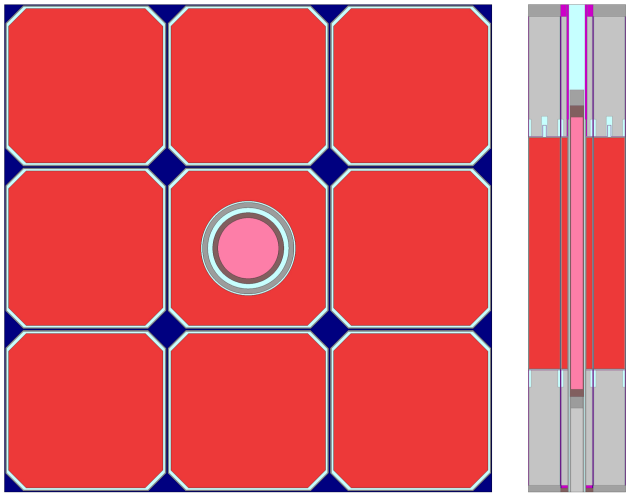

Figure 11: Control element configuration with a control rod inserted.

TREAT control rods have been shown [24, 25] to be quite problematic and can greatly influence the reported power level. Serpent simulations were performed for two different control rod settings, for Control/Shutdown and Transient rods swapped from fully withdrawn configurations to establish critical at the same power. Rod configurations are listed in Table 8 for the two configurations; rod positions (heights) are measured as the distance from the fully inserted position. The travel of all rods was illustrated earlier in Fig. 5. Here we sought to characterize extremes between rod postions, so we adopted the A and B rod bank configurations described in Table 1. The B configuration used for the Item 1 measurement had the Control/Shutdown bank fully withdrawn; the B* configuration used for measurement of Wire 6 had the Control/Shutdown bank inserted 25 cm. Although this may be required for reactivity control in the half-slotted core, we are able to better assess extreme limits assuming configuration B for these calculations.

Table 8: Positions for Control Rod Configurations A and B

Control Rod Configuration	Control/ Shutdown Rod Position	Transient Rod Position
A	55.9 cm (22.01 in)	Fully withdrawn @ 101.6 cm (40 in)
B	Fully withdrawn @ 147.3 cm (58 in)	47 cm (18.5 in)

Tables 9 and 10 provide the change in detector power readings between rod configurations A and B, for steady state and transient detector locations,

Table 9: Differences in Steady State Detector Readings as a Function of Control Rod System Configuration at a Constant Power

Startup & Steady State Detector Locations	Rod Exchange (Configuration A to B)		Temperature Change (274K to 700K, rod configuration B		Combined Effect (274K, A to 700K, B)	
	Percentage Change	1σ uncertainty (%)	Percentage Change	1σ uncertainty (%)	Percentage Change	1σ uncertainty (%)
West Face, Upper Position	-23.32	0.03	19.30	0.05	-7.58	0.03
West Face, Lower Position	-16.14	0.03	19.95	0.04	1.11	0.04
South Face, Upper Position	33.24	0.05	20.51	0.04	58.78	0.06
South Face, Lower Position	21.93	0.04	20.64	0.04	46.00	0.05

Table 10: Differences in Transient Detector Readings as a Function of Control Rod System Configuration at a Constant Power

Transient Detector Locations	Rod Exchange (Configuration A to B)		Temperature Change (274K to 700K, rod configuration B		Combined Effect (274K, A to 700K, B)	
	Percentage Change	1σ uncertainty (%)	Percentage Change	1σ uncertainty (%)	Percentage Change	1σ uncertainty (%)
NW Corner, Upper Position	2.64	2.37	8.62	2.49	11.93	2.59
NW Corner, Lower Position	0.73	2.35	6.23	2.44	9.97	2.57
NE Corner, Upper Position	3.68	2.35	5.54	2.33	8.61	2.44
NE Corner, Lower Position*	5.53	2.42	8.56	2.44	11.96	2.55
SW Corner, Upper Position	12.50	3.42	10.16	3.26	21.24	3.72
SW Corner, Lower Position	8.73	3.41	11.19	3.37	22.07	3.82
SE Corner, Upper Position	8.50	3.38	14.41	3.51	18.73	3.69
SE Corner, Lower Position	4.50	3.28	12.93	3.56	14.33	3.59

*No detectors are currently located in this position.

respectively. As seen in the second and third columns, under heading *Rod Exchange*, the effects of the control rods are substantial for the steady state chambers. As with temperatures, the cadmium-filtered transient detectors see less of an effect; however, as will be discussed below, for rod repositioning the cadmium filter on the transient detectors is not the cause of this behavior. Also note that for this comparison, the two southern corners appear to be more sensitive to the change in control rod configuration than the northern

corners. The next pair of columns, under *Temperature Change*, show the effect of temperature change on rod state B. Here the two southern corners are clearly more sensitive to the change in temperature than the northern corners. Finally, the last two columns, under *Combined Effect*, show the effect of simulateous changes from 274K and rod configuration A to 700K and rod configuration B; the net effect also most pronounced in the southern lobes, especially for the steady state detectors in Table 9. One reason for this behavior is due to the lack of fuel in the northern half of the core, which tilts the flux toward the south. Both Serpent and MAMMOTH calculations show a U shaped fission distribution around the experiment, peaked to the south. This is illustrated in Fig. 12, where the U shape is the lighter region centered around the experiment location. However, the most significant effects result from the control rod position which the two detector locations (south and west) face; southern detector locations face control/shutdown rods while western locations face transient rod locations (see Fig. 10 for the locations of the rod sets). Hence western detectors see a negative relative change and southern detectors see a corresponding positive change in moving from Configuration A to B. Both see a similar response to temperatures, with southern lobes slightly more sensitive to temperature. However, when the two are combined, the negative effect of rod position changes offsets the positive effect of temperature changes for west-face detectors. On the other hand, southern face detectors see an additive effect from rod positions and temperatures, and are much more sensitive to both effects.

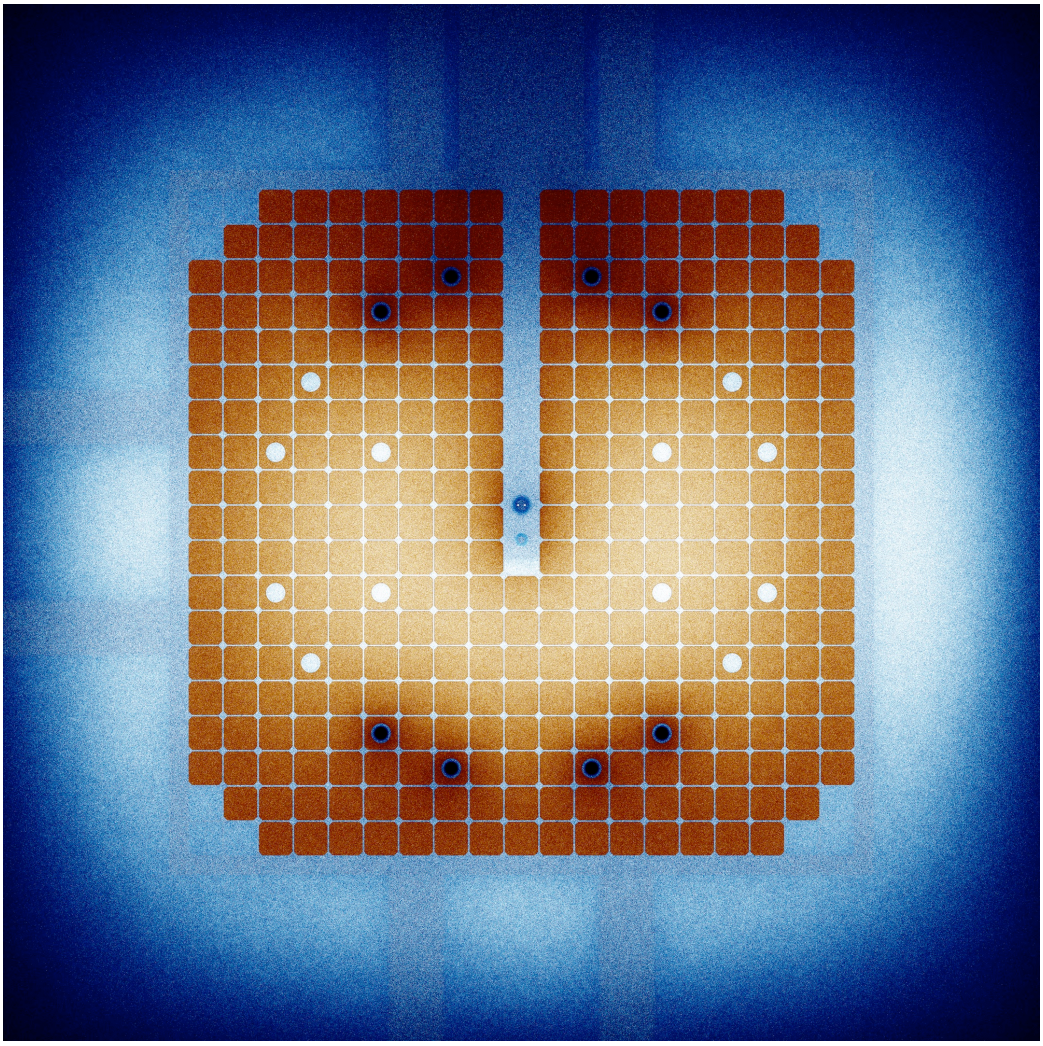

Figure 12: Serpent flux plot for fluxes averaged over the height of the fuel. The color scheme consists of *hot* shades of red and yellow, representing relative fission power, and *cold* shades of blue, representing relative thermal flux

Unfortunately, there is not much that can be done to decrease the effect of the control rod positions on the flux measured at a fixed detector location by adding filters. This is due to a nearly constant shift in the spectral plot from one rod configuration to another, as computed using Serpent and plotted in

Fig. 13, which shows the spectrum seen at the DIS-Linear detector location for the two rod configurations. The differences are somewhat diminished by the logarithmic scale; Fig. 14 shows the ratio between these two flux spectra, showing a roughly 30% difference between fluxes is seen for two rod configurations at the same power.

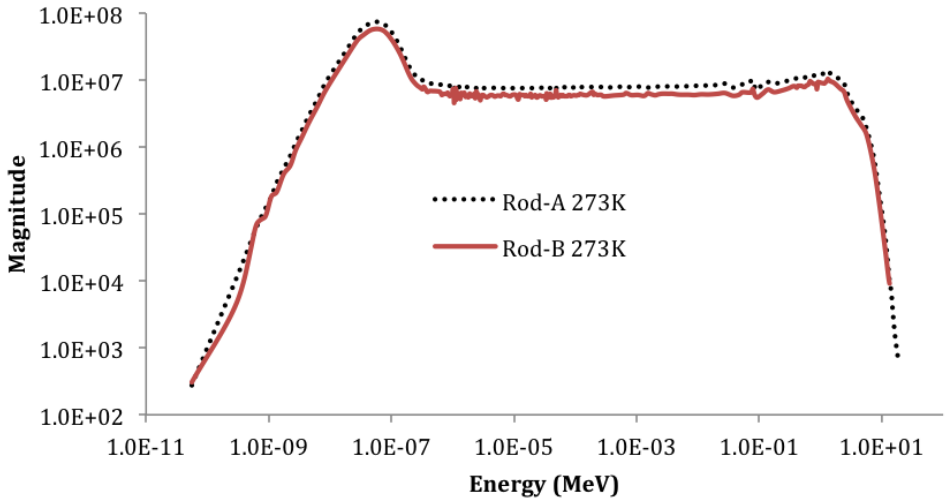

Figure 13: Flux spectra at DIS-Linear location as a function of control rod position

Because TREAT Compensation rods are always removed for measurements, configurations A and B effectively represent the two extremes for control rod positioning. Hence, 30% would be an upper bound to error in power determination as a result of rod position. Indeed, Table 9 show a maximum 33.24% change at the DIS-Linear position in the south upper slot. Note that while these calculations are indicative of upper bounds on temperature and rod position effects, taking a bounding approach can be unrealistic and serve to hide other issues. For example, for a core at 700K, temperature

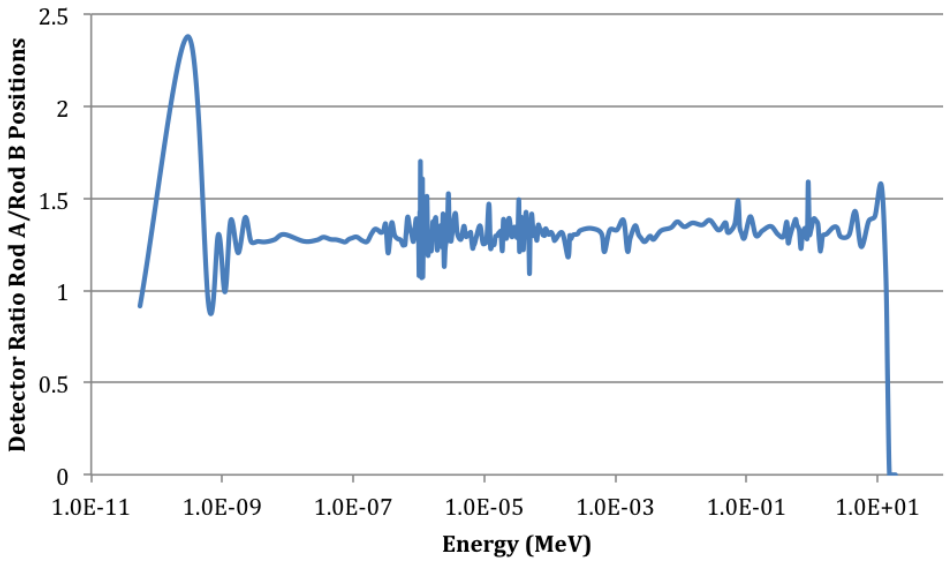

Figure 14: Ratio of flux spectra at DIS-Linear location for rod configurations A and B

feedback effects would make the core subcritical. In actual operation, (at least) one set of control rods would need to be withdrawn to compensate for temperature effects. This in turn would have an effect on detector readings. That effect could be larger than the effects reported in Tables 9 and 10. This effect should be studied in future work; however, our intent here was to illustrate the **potential** error that could be introduced due to inappropriate calibration measurements.

4.6. Challenges in Simulating Measurement Conditions.

To be able to simulate the uncertainty introduced by differences in both temperature and control rod positions, calculations must be referenced to the simulation of a specific rod and temperature measurement, i.e. the heat

balance configuration where the power calibration was actually performed. In the case of the M8 calibration series there were two heat balances, one in 1990 and another in 1992, with significant time elapsed between heat balances and actual calibration measurements, allowing for instrument drift and small changes in the core configuration due to other activities (the Argonne NPR calibration (AN-CAL) experiments [27] were performed in 1991-1992, requiring significant reconfiguration of the core). However, the greatest challenge is in knowing the actual temperature distribution of the reactor, since most of the log sheets do not report a temperature of the core but instead report a temperature of the air. Our calculations assumed a uniform core temperature for lack of better data, although we know that the temperature distribution would have the same shape as the power distribution. Using MAMMOTH it will be possible to calculate a temperature distribution, but that temperature prediction itself has not been validated and its uncertainties therefore not quantified. In future operations we hope to be able to better determine the temperature distribution for a reference calculation, through a combination of measurements and validated calculations.

4.7. Summary for Estimated Uncertainties in Core Power Measurements

Table 11 provides a summary of the estimated uncertainty in core power from the results of the above subsections. Note that these uncertainties are principally limited to steady state conditions; at this time it is difficult for us to assess effects on transient measurements, where rod positions and

Table 11: Estimates of Power Measurement Uncertainties

Source of Bias and Uncertainty	Approximate Magnitude of Uncertainty
Heat Balance	$<\sim 1\%$
Transient detectors in lower ranges during calibration	Unknown
Human Control	$<1\%$
Temperature	0 - $\sim 20\%$ †
Control Rods	0 - $\sim 30\%$ †

† Depends on deviation from state of reference measurements.

temperatures change with time and will not correspond to the calibration conditions. Temperature and control rod effects should be manifest as a quantifiable bias, but with some associated uncertainty in the bias. It is important to note that the large uncertainties on temperature and control rod effects represent what we estimate are bounding limits. Experimentalists clearly were aware of these effects, and it does appear that calibration (or calibration curves) were used to correct for rod and temperature effects to reduce the error. However, data is largely lacking to prove to this assertion.

5. APPLICATION OF UNCERTAINTIES IN PCF CALCULATIONS

Table 1 in Section 2 shows measured data and the resulting PCF values from these measurements. A Serpent 2 model was developed for the core with the M8-CAL calibration vehicle and flux monitor wire modeled to simulate these measurements. Figure 15 illustrates the core region of the Serpent model at the core mid-plane with the calibration vehicle inserted. The vehicle, in the center, contains two cylinders. The lower cylinder is a mockup of the flow tube that would be present in the M8 experiment. The upper set of nested cylinders is the experiment region; the flux wire is located in the center of this region. This model was developed to generate cross sections for the MAMMOTH model [14], but was also used to perform simulations of flux wire activation for the M8-CAL experiments described in [20]. Results, however, were not in as good agreement with measured data as would be desired. The results of the initial Serpent calculations, for items 1, 2, 5 and 6, are provided in Table 12, and range from -3% and -25% in error/.

It was observed that for the three low-enrichment wires the calculated PCF values are almost identical, while differences are seen in the measured PCFs. For identical composition wires loaded in the same location in the core, an identical PCF should be obtained, within experiment uncertainties. This observation actually led to the assessment of uncertainties reported in the previous sections in an effort to understand the relationships between indicated and actual powers as a function of temperature and control rod

location. With this knowledge, it is possible to estimate biases in indicated powers to correct the measured PCFs to actual values for the purposes of validation.

For each of the four cases listed in Table 12, two calculations were performed: the first at the conditions of the heat balance measurement (core-

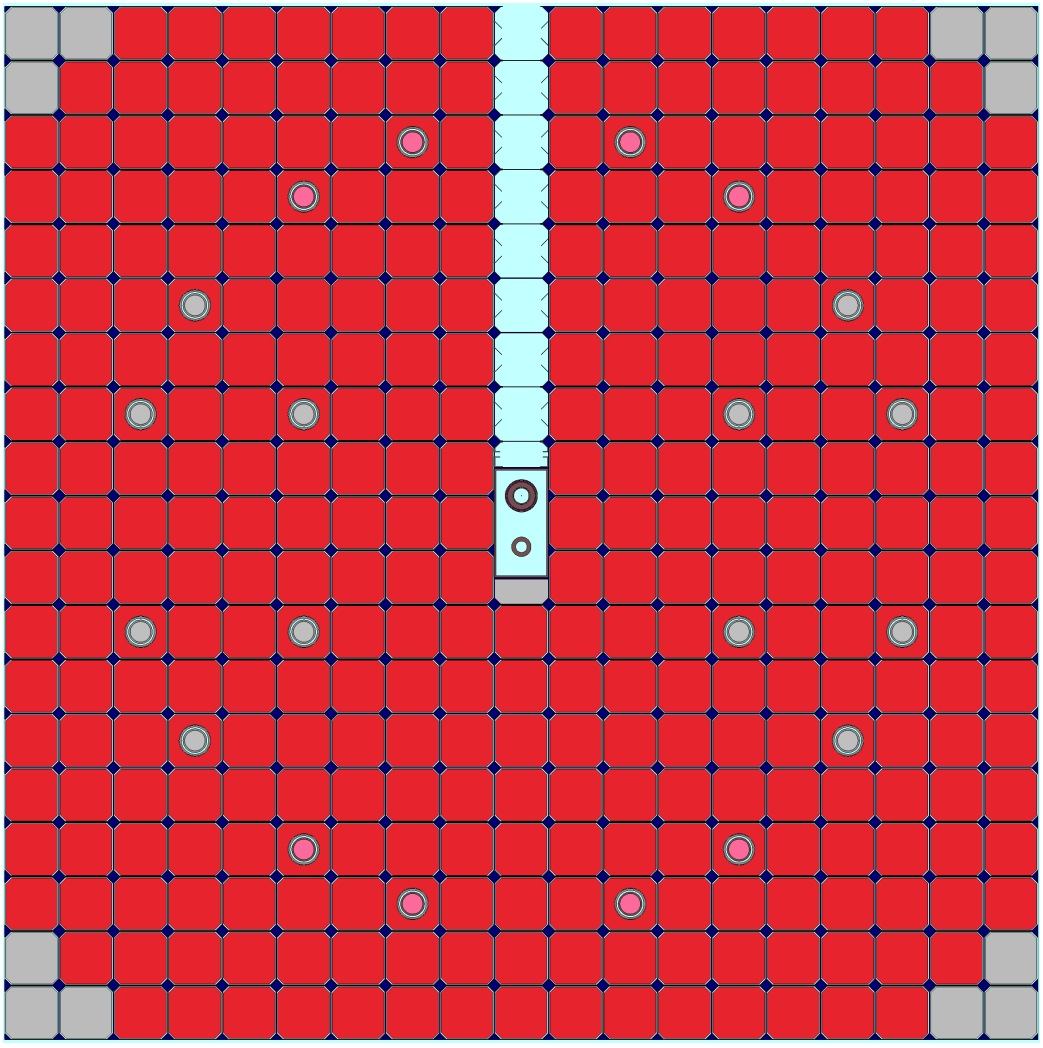

Figure 15: Serpent model of the M8-CAL configuration for TREAT.

Table 12: Initial Serpent Predictions of Power Coupling Factors from M8-CAL Measurements

Item No. (From Table 1)	Wire ID	Measured PCF ($\frac{Peak\ f/g^{235}U}{MJ}$) (x 10^{12})	Predicted PCF ($\frac{Peak\ f/g^{235}U}{MJ}$) (x 10^{12})	Error (%)
1	L91-8-10	1.79	1.338	-25.3
2	L91-60-1	1.40	1.323	-5.50
5	H91-8-1	0.503	0.488	-2.98
6	L91-8-16	1.84	1.378	-25.1

averaged temperature and rod positions); the second at the conditions reported for each of the calibration runs. The response of the simulated DIS-Linear detector position was recorded for each. The ratio of the calculated response of the heat balance run to the calculated responses of the individual calibration runs was used to adjust the calculated PCFs to account for temperature and control rod effects. In other words, the bias introduced by temperature and control rod effects was estimated by simulation of the core.

$$PCF_{adjusted} = \frac{No.\ fissions\ calculated\ in\ wire}{Calculation\ at\ documented\ power} \times \frac{Detector\ response\ at\ heat\ balance\ run}{Detector\ response\ at\ calibration\ run}, \tag{16}$$

or more simply,

$$PCF_{adjusted} = PCF_{calculated} \cdot B, \tag{17}$$

where B = Bias Factor = $\frac{Detector\ response\ at\ heat\ balance\ run}{Detector\ response\ at\ calibration\ run}$.

Table 13 lists bias factors calculated for the four calibration measure-

ments, along with adjusted PCFs obtained using Eq. 17. The adjusted PCF values are in very close agreement with the reported values, well within the overall measurement uncertainties described in previous sections. Note however that here we have calculated a bias term to adjust the calculated PCF values to those that were reported based on biased power readings. The agreement here indicates that the calculated values correctly reflect the **true** PCF values. For a computational simulation, it is much easier to calculate the PCF than it is to measure, since the calculation provides a solution normalized to the input core power, and input parameter. Thus the simulated power does not need to be inferred from external detectors. It must be recognized that for all PCF *measurements*, as reported in Table 1, the PCF was not actually measured. It was calculated based on measured fissions and a detector **current** that, as we have demonstrated, is not likely calibrated to the true power at the time of the measurement.

Table 13: Adjusted Power Coupling Factors from M8-CAL Measurements and Serpent Calculations

Item No.	Wire ID	Measured PCF ($\frac{Peak\ f/g^{235}U}{MJ}$) (x 10^{12})	Predicted PCF ($\frac{Peak\ f/g^{235}U}{MJ}$) (x 10^{12})	Bias Factor, B	**Adjusted PCF ($\frac{Peak\ f/g^{235}U}{MJ}$) (x 10^{12})**	Error (%)
1	L91-8-10	1.79	1.338	1.300	**1.740**	-2.8
2	L91-60-1	1.40	1.323	1.058	**1.400**	0.0
5	H91-8-1	0.503	0.488	0.998	**0.487**	-3.2
6	L91-8-16	1.84	1.378	1.364	**1.880**	2.2

However, it is important that core power normalization be performed correctly. By default, Serpent defaults to a power conversion factor of 202.27

MeV deposited in the core per fission. For ^{235}U fission, 180.5 MeV of recoverable energy is released instantaneously and 14.6 MeV is released from decay of fission products. Per fission event, approximately 2% ($\sim$4 MeV) of additional energy comes from non-fission events in the fuel, e.g., (n,γ), (n,2n), etc. for a total of around 200 MeV/fission [28]. This value is based on steady state operation with all fission product decay heat in equilibrium.

However, because TREAT is so small, a significant fraction of the energy per fission is deposited outside the core by leakage from the core region of both neutrons and gammas. TREAT operations historically assumed 173 MeV/fission for instantaneous release [3]. This value has been confirmed recently by MCNP5 [29] calculations. In addition, an additional 9 MeV/fission of decay heat was assumed for decay of short-lived fission products (based on 60 seconds of operation) for a total of 182 MeV/fission of recoverable energy in the core. This value was used to scale the calculated flux to the input core power. It should be noted, however, that it is not clear if this underestimates power from longer-term (steady-state) operation from LLSS and heat balance operations. Thus this is another source of uncertainty, although only for the core simulation (flux normalization), not for the measurements.

The bias factors for wires 1 and 6 are the largest, on the order of 1.33. Note from Table 1 these measurements were made in control rod state B. These two measurements may contain offsetting errors, as the wire 1 measurement was made with the full-slot core; measurement 6 was close to the B state but not quite the same. Nevertheless the heat balance was performed

with control rods in arrangement A. Hence a large part of the bias is due to the altered control rod position, perhaps as large as on the order of 25%, consistent with earlier observations. Wire 2 was measured with control rods in configuration A, with only temperature effects, on the order of 6%. Similarly for wire 3 the temperature effect is negligible.

This consistency of the measured data with bias-adjusted calculations gives us confidence in our ability to calculate PCFs. However, confidence and validation are not the same thing, and it is difficult to call this a validation of the method, because of the need to introduce bias factors that were calculated, not measured. Instead, validation calculations must be performed in a manner similar to the actual measurements, by performing simulation of detector responses for heat balance, LLSS and transient runs.

6. SUMMARY

Study of the behavior of the INL Transient Test Reactor based on historical data is ongoing. With new and advanced 3-D methods for simulation of core operations (steady state and transient) there is a need to obtain data that can validate these methods. Unfortunately, data obtained in measurements performed before 1994 is often incomplete, and measurement campaigns certainly weren't designed to validate 3-D transient multiphysics methods. The MAMMOTH reactor multiphysics application has been shown to be able to closely simulate core transient behavior as reported by transient detectors within the uncertainty of those measurements [12]. However, key to successful use of the tool for support of experiment design and testing is the ability to simulate events occuring with an experiment vessel. To date this has been a significant challenge; hence this research has been undertaken to determine potential uncertainties in previous measurement methods, and to quantify biases and uncertainties associated with those measurements. This work has demonstrated that by calculation of biases for low-level steady-state conditions (resulting from temperature and control rod positioning effects relative to the detector calibration state), it is possible to closely reproduce measured power coupling factors for sample fission wires, with and without a neutron filter. However, because the estimated biases are themselves calculated based on some assumptions, it would be inappropriate to use those results as part of a validation process. Our conclusion, therefore, is that instead of trying to calculate actual PCFs, future work should be based on the

actual measurement approach, to try to reproduce the reported PCFs solely based on simulations of detector responses.

This approach in itself offers other simulation challenges. Calculations to this point assumed steady state operation, whereas LLSS measurements are known to have been performed with temperature increases and control rod rod motion. Figure 16 shows the measurement log for the H91-8-1 HEU wire (item 5 in Table 1). The experiment was run for approximately two hours (no indication of ramp-up time, as discussed in Sec. 3.2.2). Based on this operation time, the core had not achieved an equilibrium temperature. The record shows a final temperature of 115 C; presumably the starting temperature was 20 C. The positions (in inches) of each of the individual rod sets are provided (one pair of rods is attached to each rod drive) for the Control/Shutdown rods. The difference in the beginning and ending sets was approximately 11.4 cm (4.5 in). Assuming the reactor was operated at a constant power on the DIS-Linear chamber, a simulation would have to operate in a transient mode in which temperature increase and control rods are moved to maintain a constant reaction rate in the detector. Simulateously matching power, the temperature change and the rod motion may be a challenge, but allowance would need to be made for uncertainties.

One observation that can be made from the simulations discussed earlier is that while the detectors were shown to be sensitive to both temperature and control rod position. However, the PCF values calculated with different temperatures and rod positions, with a full slot and half slot core, all remain

at about the same value. It is possible that the PCF value has much less sensitivity to rod position nor core temperature than has been expected. Future simulations to study this hypothesis are planned. Future plans also include transient simulations. While Serpent 2 has recently added transient capabilities [30], the computational effort required to reduce uncertainties to on the order of 3% for transient detector locations is significant (2.5×10^{10} neutron histories); on the order of 1000s of simulations (weeks to months) would be required to complete a 10 second transient. And although MAMMOTH is able to perform full core TREAT transient simulations in an acceptable time period (minutes to hours), current modeling efforts have performed 3-D simulations only out to the edge of the permanent reflector. Cross sections calculated for the permanent reflector region, while having little effect on power transients, are known to be in error by comparison with Serpent reaction rates. These issues must be addressed before proceeding to modeling of

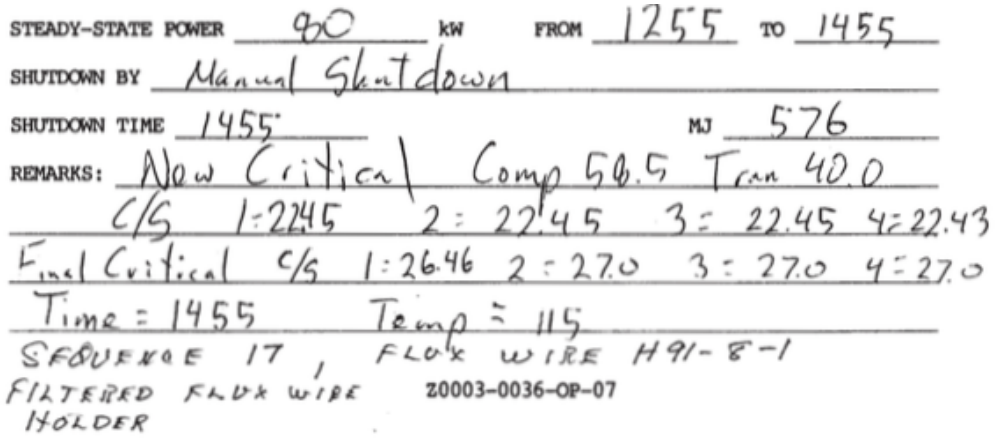

Figure 16: Measurement data for the H91-8-1 HEU wire LLSS irradiation.

the biological sheild and reflector.

It is important to recognize that the error in a predicted PCF (recall that PCFs are not directly measured) is a combination of the error in the numerator, i.e., the determination of the number of fissions that were determined for a wire or fuel pin, and the error in the denominator, i.e., the estimated core power. These two terms are independent. Section 3 discussed potential source of error, which were summarized in Table 2. This work concluded that the error in fission estimates was likely on the order of $\pm 5\%$. The error in core power is completely independent of the fission measurement, and was discussed in Sect. 4. Table 11 shows that errors other than temperature and rod effects are quite small, but that temperature and control rod effects could potentially have a large effect on core power determination. Careful calibration could reduce the magnitude of this error, but it is likely that the power estimate is in error by on the order of 5% to and perhaps up to 10%. It is doubtful that this could be improved on using existing techinques, but advanced instrumentation and measurement techniques might be able to reduce the error in power measurement. The clear solution to the problem, however, is to eliminate the use of PCF and TCF corrections completely. If advanced modeling methods are able to accurately predict experiment behavior, then the need for calibration measurements and PCF/TCF calculations are eliminated. This would significantly reduce the cost of operations and increase experiment throughput. However, such advanced methods will be difficult to deploy until they have been validated by experimental mea-

surement data. Hence the plan will be to resume operations based on the previous power calibration measurements. However, measurements will be performed that consider three dimensional methods for the purpose of code validation. It is expected that MAMMOTH deployment at TREAT will be a migrational transition as experience with the core is gained and high quality three-dimensional data becomes available.

TREAT is expected to be returned to service for testing and calibration in late 2017, with a broad series of physics measurements beginning in early 2018. Included in these measurements will be 3-D temperatures, 3-D flux, fission wire and spectral measurements (in the experiment location), each as a function of temperature. core air flow rates, rod worths, β_{eff} and λ, along with possible neutron transmission measurements. In addition, initial testing will repeat a subset of M8-CAL measurements in the current calibration vehicle, followed by the Multi-SERTTA calibration vehicle (Multi-SERTTA-CAL, or MS-CAL), in preparation for the subsequent Multi-SERTTA fuel test program [31]. The current design of the MS-CAL vehicle contains Micro-Pocket Fission Detectors (MPFDs) [32], which will allow real-time measurements of the flux in the core. MPFDs are still prototypical so early measurements will be tests of the devices themselves, but it is expected that these detectors will eventually provide valuable data for not just code validation but also for experimental measurements themselves.

The data obtained from all of the above measurements, combined with ongoing improvements in MAMMOTH transient simulation capabilities, are

expected to provide needed code validation for NQA-1 Quality Level 1 certification of MAMMOTH for eventual safety analysis support for TREAT, and provide the first 3-D full core transient analysis capability to ever be applied in TREAT operations, experiment and expeiment design applications.

7. ACKNOWLEDGEMENTS

This work was supported by the U.S. Department of Energy, Office of Nuclear Energy, Advanced Modeling and Simulation Program, under DOE-NE Idaho Operations Office Contract DEAC07-05ID14517.

8. BIBLIOGRAPHY

[1] G. A. Freund, H. P. Iskendarian and D. Okrent, TREAT, a Pulsed Graphite-Moderated Reactor for Kinetics Experiment, in: Proc. 2nd United Nations Int. Conf. on the Peaceful Uses of Atomic Energy, Vol. 10, Geneva, Switzerland, 1958, pp. 461–475.

[2] U.S. Department of Energy, Resumption of Transient Testing Capability, http://energy.gov/ne/articles/resumption-transient-testing (April 15 2013).

[3] D. Okrent, C. Dickerman, J. Gasidlo, D. O'Shea, D. Schoeberl, The Reactor Kinetics of the Transient Reactor Test Facility (TREAT), Tech. Rep. ANL-6174, Argonne National Laboratory (1960).

[4] F.N. Gleicher, J. Ortensi et al, The Coupling of the Neutron Transport Application Rattlesnake to the Fuels Performance Application BISON, in: International Conference on Reactor Physics (PHYSOR 2014), Kyoto, Japan, 2014.

[5] R. Magazine, 2014 R&D 100 Award Winners, "`http://www.rdmag.com/award-winners/2014/08/2014-r-d-100-award-winners`.

[6] D. Gaston, C. Newman, G. Hansen, D. Lebrun-Grand'e, MOOSE: A parallel computational framework for coupled systems of non-linear equations, Nucl. Eng. Design 239 (1768-1778).

[7] Y. Wang, Nonlinear Diffusion Acceleration for the Multigroup Transport Equation Discretized with SN and Continuous FEM With Rattlesnake, in: Proceedings of the International Conference on Mathematics, Computational Methods & Reactor Physics (M&C 2013), Sun Valley, Idaho, USA, ID, 2016.

[8] R.L. Williamson et al., Multidimensional Multi-physics Simulation of Nuclear Fuel Behavior, Jou. Nucl. Mat. 423 (149–163).

[9] J. D. Hales et al., Advanced multiphysics coupling for lwr fuel performance analysis, Annals of Nuclear Energy 84 (2015) 98–110.

[10] D. Andrs et al., RELAP-7 Level 2 Milestone Report: Demonstration of a Steady State Single Phase PWR Simulation with RELAP-7, Tech. Rep. INL/EXT-12-25924, Idaho National Laboratory (2012).

[11] J. Ortensi et al., Initial Testing of the Microscopic Depletion Implementation in the MAMMOTH Reactor Physics Application, Tech. Rep. INL/EXT-16-39930, Idaho National Laboratory, Idaho Falls, ID (Sept. 2016).

[12] J. Ortensi, M. D. DeHart, F. N. Gleicher, Y. Wang, S. Schunert, A. L. Alberti, T. S. Palmer, Full Core TREAT Kinetics Demonstration Using Rattlesnake/BISON Coupling Within MAMMOTH, Tech. Rep. INL/EXT-15-36268, Idaho National Laboratory (2015).

[13] M. D. DeHart, J. Ortensi, F. N. Gleicher, Y. Wang, S. Schunert, Research in Support of TREAT Kinetics Calculations Using Rattlesnake/BISON Coupling within MAMMOTH, in: PHYSOR 2016: Unifying Theory and Experiments in the 21st Century, American Nuclear Society, Sun Valley, Idaho, USA, 2016.

[14] J. Ortensi, A. Alberti, Y. Wang, M.D. DeHart, F.N. Gleicher, S. Schunert, T.S. Palrmer, Methodologies and Requirements for the Generation of Physics Data Inputs to MAMMOTH Transient Simulations in Support of the Transient Reactor Test Facility, Tech. Rep. NL/EXT-15-36265, Idaho National Laboratory (September 2015).

[15] J. Ortensi, S. Schunert, Y. Wang, B. A. Baker, F. N. Gleicher, M. D. DeHart, A Neutron Streaming Problem to Test Rattlesnake Methods for TREAT, INL/CON-16-39358, in: Proceedings of the ANS 2016 Winter Meeting, American Nuclear Society (To be published), Las Vegas, NV, 2016.

[16] A. L. Alberti, T. S. Palmer, J. Ortensi, M. DeHart, Steady State Modeling of the Minimum Critical Core of the Transient Reactor Test Facility, in: International Conference on Reactor Physics (PHYSOR 2016), Sun Valley, Idaho, USA, 2016.

[17] J. Leppänen et al., The Serpent Monte Carlo code: Status, development and applications in 2013, Ann. Nucl. Energy 82 (2015) 142–150.

[18] M.B. Chadwick et al., "endf/b-vii.1: Nuclear data for science and technology: Cross sections, covariances, fission product yields and decay data", Nucl. Data Sheets 112 (12) (2011) 2887–2996.

[19] National Instruments Corporation, Labview (32 bit) 2015, http://www.ni.com/download/labview-development-system-2015/5308/en/ (2015).

[20] T. H. B. W. R. Robinson, The M8 Power Calibration Experiment (M8CAL), Tech. Rep. ANL-IFR-232, Argonne National Laboratory (May 1994).

[21] J. D. Bess, M. D. DeHart, Baseline Assessment of TREAT for Modeling and Analysis Needs, Tech. Rep. INL/EXT-15-35372, Idaho National Laboratory (2015).

[22] B. A. Baker, M. D. DeHart, J. Ortensi, Y. Wang, F. N. Gleicher, S. Schunert, Recommendations for TREAT Historical Data to Validate MAMMOTH, Tech. Rep. INL/EXT-16-38059, Idaho National Laboratory, Idaho Falls, Idaho (Jan 2016).

[23] A. D. Volpi, R. J. Pecina, R. T. Daly, D. J. Travis, R. R. Stewart, E. A. Rhodes, Fast-Neutron Hodoscope at Treat: Development and Operation, Nucl. Technol. 27 (3) (1975) 449–487.

[24] G. Klotzkin, R. W. Swanson, P. Hart, L. J. Harrison, Time Dependence

of Test Fuel Power Coupling During Transient Reactor Test Facility Irradiation Experiments, Nuc. Sci. Eng. 86 (1984) 206–218.

[25] D. Kontogeorgakos, H.M. Connaway, A.E. Wright, Temperature Dependence of Test Fuel Power Density and Core Energy during Transient Reactor Test Facility (TREAT) Irradiation Experiments", , tx, june 7-11 2015., in: Proceedings of the ANS 2015 Annual Meeting, "Nuclear Technology: An Essential Part of the Solution", American Nuclear Society, San Antonio, TX, 2015.

[26] D. R. Burrows, F. L. Hooper, G. Klotzkin, Analysis of Recent TREAT Heat Balances, [Interoffice Memorandum] (Feb 11 1980).

[27] W. Robinson, R. Page, A. Wright, TREAT-NPR Calibration Experiment ANCAL, Tech. Rep. ANL/NPR-92/11, Argonne National Laboratory (Nov 1992).

[28] D. Bodansky, Nuclear energy : principles, practices, and prospects, Springer : AIP Press, New York, 2010.

[29] F. B. Brown et al., MCNP Version 5, Tech. Rep. LA-UR-02-3935, Los Alamos National Laboratory (2002).

[30] J. Leppänen, Development of a dynamic simulation mode in serpent 2 monte carlo code, in: Proceedings of the International Conference on Mathematics and Computational Methods Applied to Nuclear Science

and Engineering, M&C 2013, American Nuclear Society, Sun Valley, ID, 2013.

[31] N. E. Woolstenhulme et al., Capabilities Development for Transient Testing of Advanced Nuclear Fuels at TREAT, in: Proceedings of Top Fuel 2016, American Nuclear Society, Boise, ID, 2016.

[32] V. K. Patel, M. A. Reichenberger, J. A. Roberts, T. C. Unruh, D. S. McGregor, MCNP6 Simulated Performance of Micro-Pocket Fission Detectors (MPFDs) in the Transient REActor Test (TREAT) Facility, Annals of Nuclear Energy 104 (2017) 191 – 196. doi:http://doi.org/10.1016/j.anucene.2017.02.017.